Journal of the Franklin Institute 361 (2024) 283–300

Contents lists available at ScienceDirect

Journal of the Franklin Institute

journal homepage: www.elsevier.com/locate/fi

# A unified methodology for the power efficiency analysis of physical systems

Davide Tebaldi *, Roberto Zanasi

*University of Modena and Reggio Emilia, Via Pietro Vivarelli 10, - int. 1, Modena, 41125, Italy*

ARTICLE INFO

*Keywords:*
Electromechanical system
Power efficiency
Formal concept analysis
Mathematical model
Mechanical system
Efficiency map

ABSTRACT

In this paper, the problem of power efficiency evaluation for $n$-ports physical systems is investigated. The efficiency analysis that we perform highlights the necessary and sufficient conditions for the system to be passive, and outlines the guidelines for the efficiency maps computation. After addressing the problem from a formal point of view, the analysis is deepened for the case of two-ports linear and nonlinear physical systems, and for the cases of three and four-ports linear systems. The efficiency analysis and the computation of the efficiency maps are addressed as a function of the power variables characterizing all the energetic ports of the considered systems. Furthermore, the salient properties of the efficiency are highlighted and discussed. The theoretical analysis which is developed is then applied to some physical systems of interest for industries and engineers working in the electromechanical, hydraulic and automotive fields: a DC electric motor driving an hydraulic pump for the two-ports systems class, a single-stage planetary gear set for the three-ports systems class, and a Ravigneaux planetary gear set for the four-ports systems class.

## 1. Introduction

The word efficiency is largely employed in the literature to describe several concepts, which allow to evaluate the performances of a physical system. A first possible use of this word is related to the world of series machines in production lines. In this case, the concept of efficiency aims at capturing the impact that downtimes, caused by a failure for example, have on the throughput of the series machines system. This subject is discussed in [1], where the authors focus on the estimation of the efficiency of series machines in production lines. Since the awareness of global warming has been largely increasing in recent years, another important use of the word efficiency is related to the concept of energy or power efficiency. The potential reduction in the energy consumption brings several advantages, both from the point of view of the environmental sustainability and from the point of view of the economic return.

In general, a complex physical system can be defined as the combination of several physical subsystems, interacting with each other and with the external world through energetic ports, also called power sections. This interaction can either take place within the same energetic domain or between two different energetic domains [2]. The performance evaluation of a complex physical system from the energetic point of view includes both its transient behavior, which depends on the dynamic elements and affects the trajectories movement in the system state–space, and the power efficiency evaluation in different operating points, affected by the dissipative terms within the system. The first evaluation is addressed in [3], where a new control algorithm is proposed to compensate speed fluctuation in the constant velocity motor present in a hybrid machine system. In this paper, the focus is on

* Corresponding author.
*E-mail addresses:* davide.tebaldi@unimore.it (D. Tebaldi), roberto.zanasi@unimore.it (R. Zanasi).

https://doi.org/10.1016/j.jfranklin.2023.12.004
Received 16 April 2021; Received in revised form 4 June 2023; Accepted 4 December 2023
Available online 10 December 2023

the second aspect, that is the power efficiency evaluation of different types of physical systems, so as to be able to build their efficiency map. This is a first necessary step to derive the overall efficiency map of a complex physical system. With reference to the global warming problem, an example of air pollution source is represented by transportation systems, including road transport. In such application, a lot of investigation has been carried out in the last years on Hybrid Electric Vehicles (HEVs), representing a promising solution. The term HEVs identifies those vehicles whose propulsion system contains more than one power source, typically endothermic and electric. In the context of hybrid machines definition given in [4], the considered HEVs for road transportation fall within the category of hybrid actuation systems, since more than one type of motors are present to accomplish the task. The subject of power efficiency has been largely treated in the literature in the last decades. For example, a theory of the mechanical efficiency for kinematic heat engines is presented in [5,6]. The efficiency optimization of an induction machine is addressed in [7], by minimizing the power losses defining the optimal rotor flux, whereas the efficiency maximization of wind turbines in the presence of electrical faults is addressed in [8]. The efficiency analysis of a dual active bridge bidirectional DC–DC converter using dual phase shift control is instead performed in [9], in order to derive the system efficiency maps in different operating conditions and to analyze the efficiency of a series hybrid electric vehicle including the considered converter. Electric traction motors and the associated drives are analyzed in [10], where the employment of the efficiency maps as a function of the speed/torque operating point to describe the efficiency of traction motors for HEVs is described. A similar usage of efficiency maps in the context of hybrid transmission systems is also made in [11], in order to represent the traction motor and generator efficiencies operating points as a function of the speed/torque operating point. Efficiency maps do represent a powerful tool in the automotive field for HEVs especially from a control point of view: once the most suitable architecture has been identified, see [12–15], an effective solution for the power management problem must be found. For this purpose, Model Predictive Control (MPC) is used in [16] using static and dynamic HEV models. Specifically, a quasi-static model of the electric machine is employed, which is based on the electric machine efficiency map in the different operating modes. The solution in [17] aims to make the electric machines present in the considered electric propulsion system work in the high-efficiency regions exploiting the Instantaneous Power Minimization (IPM) process. Such tools as efficiency maps are also used in [18], in order to establish an energy management strategy for a type of electric vehicles, with the aim of minimizing the motors and transmission consumed power. A rule-based energy management strategy for series–parallel hybrid bus is proposed in [19], where the efficiency map is employed to show the efficiency of the electric machines involved in the considered hybrid architecture.

Many other application examples can be found in the literature. In [20], the authors focus on the efficiency improvement of an electrically activated rotation-flow suction unit. The efficiency map creation of an hydraulic-actuator control system is presented in [21], which is used as a tool for understanding the performance characteristics of the considered system in different operating conditions. The problem of systems efficiency evaluation is instead addressed in [22], and a metric allowing to perform the evaluation of the energy system efficiency is provided. An energy efficiency evaluation system is then shown in [23], whereas two types of electric machines are taken into account so as to compare their efficiency maps in [24]. Efficiency maps establish a first qualitative and quantitative information about the considered system efficiency in all its operating conditions. Furthermore, they allow to evince the dependence of the system efficiency as a function of the power variables in the considered system energetic port, as it is done in [25] for hydraulic orbit motors for example. Other instances of systems efficiency evaluation can be found in [26,27].

The different practical examples described so far highlight how largely employed the concept of efficiency is in many industrial applications. In this paper, we approach the physical systems power efficiency evaluation using a unified approach, exploiting the system physical modeling as a backbone for the power efficiency analysis and for outlining the procedure to build the system efficiency maps. The system modeling can be made with an energetic approach using different modeling techniques, including Bond Graphs [28,29], Energetic Macroscopic Representation [28–30], and Power-Oriented Graphs [2,31]. The main characteristics of these techniques are compared in [32]. In this paper, the Power-Oriented Graphs (POG) technique is employed, for which some application examples can be found in [15,33–35].

When dealing with Power-Split HEVs, see [12–15,36], an interest arises in the class of $n$-ports physical systems, since Power-Split HEVs are a category of HEVs equipped with an $n$-ports device, typically a planetary gear set [33,34,37–40]. A schematic representation of a Power-Split HEV equipped with an $n$-ports planetary gear set is shown in Fig. 1. From the figure, it is possible to see how the different power sources and the load are connected to the different energetic ports of the planetary gear set. In the case study of Fig. 1, the ICE (Internal Combustion Engine) is connected to the first energetic port of the planetary gear set, whereas $n-2$ EMs (Electric Motors) are connected from the second to the $(n-1)$-th energetic ports. The Vehicle Transmission System, representing the load of the architecture, is connected to the $n$-th energetic port of the planetary gear set. The objective of the planetary gear set device is to split the ICE power into different parallel power paths driving the Vehicle Transmission System, thus enabling the optimization of the ICE operating point in order to minimize the fuel consumption. Different approaches for modeling planetary gear sets are present in the literature for different purposes. One of the most widespread approaches is the Lever Analogy, introduced by Benford and Leising [37], which is very suitable for system analysis. As an example, this approach is used in [36] to analyze the operating modes of the considered hybrid electric vehicle. The kinematic structure and synthesis of gear trains involving planetary gear sets is addressed in [38–40] using a graph notation. In [33,34], a new approach which allows for the systematic modeling of planetary gear sets was introduced, which is suitable for simulation and control purposes thanks to the proposed general dynamic model for any planetary gear set. The present paper focuses on the step of evaluating the physical systems power efficiency, once the modeling is performed, by building the system efficiency maps. Thanks to the proposed analysis, the efficiency map can be computed on different operating planes defined by the power variables composing each energetic port of the system. The resulting efficiency maps are interchangeable and represent a degree of freedom for the designer, who can choose the most significant energetic port

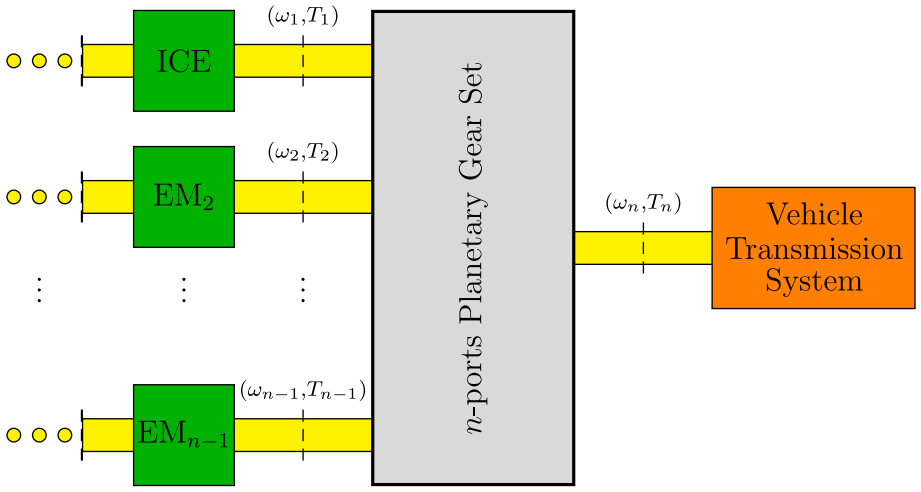


**Fig. 1.** Schematic representation of a Power-Split Hybrid Electric Vehicle.

upon which the power efficiency evaluation of the physical system to be dealt with can be based. In Power-Split HEVs, the power sources are typically connected to the energetic ports of the planetary gear set, as shown in Fig. 1. Therefore, the efficiency map of the planetary gear set can be represented and studied on the energetic port of each power source. This is important in order to account not only for the ICE and EMs efficiency when developing the energy management strategy of the vehicle, but for the planetary gear set efficiency as well.

The remainder of this paper is organized as follows. Section 2.1 summarizes the contributions of this paper with respect to our previous work, whereas Section 2.2 discusses the contributions of this work with respect to the literature and highlights the practical applications of the proposed approach. In Section 3, the definition of efficiency and its properties for the most generic case of $n$-ports physical systems are addressed. The subcases of two, three and four-ports physical systems are then addressed in Sections 4, 5 and 6, respectively. As far as two-ports systems are concerned, the efficiency map computation and analysis as a function of the power variables $(y_2, u_2)$ of the second energetic port and as a function of the power variables $(y_1, u_1)$ of the first energetic port are carried out in Section 4.1 and in Section 4.2, respectively. Section 4.3 highlights the presence of a design parameter $q$ characterizing all two-ports linear systems. The importance of this parameter is then described, as it gives the maximum value of the system efficiency in forward mode, that is when the power flow is oriented from the first to the second energetic port, and in reverse mode, that is when the power flow is oriented from the second to the first energetic port. The efficiency analysis of a new case study is then presented in Section 4.4, that is a DC motor driving an hydraulic pump both in the linear case, see Section 4.4.1, and in the nonlinear case, see Section 4.4.2. The three-ports system case study addressed in Section 5 is a single-stage planetary gear set, whereas the four-ports system case study addressed in Section 6 is a Ravigneaux planetary gear set. For the planetary gear set case studies in Sections 5 and 6, the computation of the system efficiency map on the power variables of all the system energetic ports is addressed, by also showing the different characteristics and properties that the efficiency maps exhibit. Section 7 presents the conclusions of this work, whereas the proofs of the properties are reported in the Appendix part.

## 2. Contributions of this paper

### 2.1. Contributions with respect to the previous work

The power efficiency analysis of two-ports systems has been addressed in [41,42]. In this paper, we provide the following new contributions:

(a) the extension of the efficiency analysis from the case of two-ports physical systems to the case of $n$-ports physical systems;
(b) the extension of the two-ports systems efficiency analysis as follows: (b.1) mathematical proofs are set out in greater detail, see Sections 4, 4.1 and 4.2; (b.2) a new property distinguishing between necessary/necessary and sufficient conditions for the physical system to be passive as a function of the system parameters is given (see Property 2); (b.3) the meaning and usage of the design parameter $q$ giving the maximum efficiency value for the considered physical system is deepened (see Section 4.3); (b.4) a new case study is presented (see Section 4.4), consisting in a DC motor driving an hydraulic pump. We show that the latter behaves as a two-ports system affected by nonlinearities with physical elements in three different energetic domains;
(c) the efficiency analysis of a three-ports planetary gear set typically employed in HEVs is addressed in Section 5;
(d) the efficiency analysis of a four-ports planetary gear set, called Ravigneaux planetary gear set, typically employed in HEVs is addressed in Section 6.

For the considered planetary gear sets in Sections 5 and 6, the inherent characteristics and properties they exhibit are presented and commented on.

### 2.2. Contributions and significance with respect to the literature

The literature review performed in Section 1 led us to the following considerations: (1) the concept of power efficiency is largely employed in the industrial and academic worlds to evaluate the dissipations of physical systems; (2) the most widespread way of expressing the physical systems power efficiency is through efficiency maps computed as a function of the system power variables; (3) to the best of our knowledge, the evaluation of systems power efficiency to build the efficiency maps does not refer to any unified theoretical formulation of the problem, and is rather based on evaluations made on each individual physical system under consideration.

Based on these considerations, in this paper, we share our analysis approaching the efficiency map derivation for physical systems based on a *unified formulation of the problem, applicable to different physical systems in different energetic domains*. Our intent is therefore to outline the guidelines to compute the efficiency maps as a function of the systems parameters for different categories of physical systems in different energetic domains, and to show some useful properties intrinsic of physical systems and of their efficiency maps. Our approach for automatically finding the physical systems efficiency maps starts from unifying the approach for modeling physical systems. Since the computation of the physical systems efficiency maps is still mostly done case-by-case nowadays, we believe that our approach can provide important insights on the proper way of modeling the considered physical systems in order to automatically be able to compute their efficiency maps. The use of a unified approach for finding the systems efficiency maps can not only help researchers and industrials to make their work more accessible to the entire community, but can also help them to verify the results they achieve by verifying that the obtained efficiency maps satisfy the common properties which we have found. In this paper, the main problem that we aimed to solve has therefore been the proposal of a unified efficiency analysis for the most general case of $n$-port physical systems, with the final objective of building the system efficiency maps as a function of the system parameters and to highlight some common properties that all efficiency maps share.

We then focus on two-ports linear systems first, to emphasize *the presence of a common design parameter, and to show the approach for computing the efficiency map*. Several two-ports physical systems case studies were analyzed in our previous work [41,42], and a new case study is addressed in this paper, namely a DC motor driving an hydraulic pump.

Next, the generalization to the $n$-ports systems case study we addressed in this paper has allowed us to analyze two new important case studies in the automotive field: the single-stage planetary gear set for the three-ports systems category, and the Ravigneaux planetary gear set for the four-ports systems category. For the latter physical systems, *the presence of some inherent characteristics and properties is claimed and justified, and a procedure for deriving the efficiency map on different energetic ports is given, providing an important degree of freedom for the designer*.

The generality of the proposed approach makes it applicable to different physical systems in different energetic domains which are of interest for researchers and industries working in many different engineering fields. Electromechanical devices such as DC electric motors, Permanent Magnet Synchronous Motors and electrical circuitry were addressed in our previous work [41,42], whereas important hydraulic and mechanical devices such as hydraulic pumps and different types of planetary gear sets, which are the key elements of Power-Split Hybrid Electric Vehicles, have been addressed in this paper. Furthermore, since the theoretical foundation has been established with reference to the most generic case of $n$-ports physical systems in this paper, the reader has all the tools for applying the proposed efficiency analysis to any physical system of their interest, and finally find the system efficiency maps.

## 3. Efficiency of linear physical systems

Let us consider a linear physical system $\mathbf{H}(s)$ characterized by $n$ energetic ports, or power sections, whose schematic representation is given in Fig. 2. The pairs $(y_1, u_1)$, $(y_2, u_2)$, …, $(y_n, u_n)$ denote the power variables of energetic ports 1, 2, …, $n$, respectively. The arrows located in correspondence of each energetic port define the positive orientation of the power flows: power $P_h = u_h\, y_h > 0$, $\forall h = 1, 2, \ldots, n$, if it is entering the system. Let $P_I$ denote the following set:

$$P_I = \left\{ i \,:\, P_i > 0, \forall i = 1, 2, \ldots, n \right\}, \tag{1}$$

of all the subscripts $i$ of the powers $P_i > 0$ entering the system. Let $P_O$ denote the following set:

$$P_O = \left\{ j \,:\, P_j < 0, \forall j = 1, 2, \ldots, n \right\}, \tag{2}$$

of all the subscripts $j$ of the powers $P_j < 0$ exiting the system. The state–space equations of the considered system $\mathbf{H}(s)$ are:

$$\begin{cases} \mathbf{L}\dot{\mathbf{x}} = \mathbf{A}\mathbf{x} + \mathbf{B}\mathbf{u} & \mathbf{u} = \left[u_1\ u_2\ \cdots\ u_n\right]^{\mathrm{T}}, \\ \mathbf{y} = \mathbf{C}\mathbf{x} + \mathbf{D}\mathbf{u} & \mathbf{y} = \left[y_1\ y_2\ \cdots\ y_n\right]^{\mathrm{T}}, \end{cases} \tag{3}$$

where $\mathbf{u}$ and $\mathbf{y}$ are the input and output vectors. The state–space representation in (3) is preferred over the classical state–space representation used in control system theory for linear time-invariant systems because a physical meaning can be assigned to the system matrices [2]. The *energy matrix* $\mathbf{L}$ carries the information about the energy instantaneously stored in the system, whereas the *power matrix* $\mathbf{A}$ carries the information about the power instantaneously dissipated in the system [2]. The input–output transfer matrix $\mathbf{H}(s)$ of system (3) is given by $\mathbf{H}(s) = \mathbf{C}(\mathbf{L}\,s - \mathbf{A})^{-1}\mathbf{B} + \mathbf{D}$. The system is supposed to be operating in steady-state conditions, in order to be able to build the efficiency map providing the system efficiency in each operating point. The static transfer matrix $\mathbf{H}_0 = \mathbf{H}(s)|_{s=0}$ relates the input vector $\mathbf{u}$ and the output vector $\mathbf{y}$ as follows:

$$\mathbf{y} = \mathbf{H}_0\,\mathbf{u}, \qquad \mathbf{H}_0 = -\mathbf{C}\mathbf{A}^{-1}\mathbf{B} + \mathbf{D}. \tag{4}$$

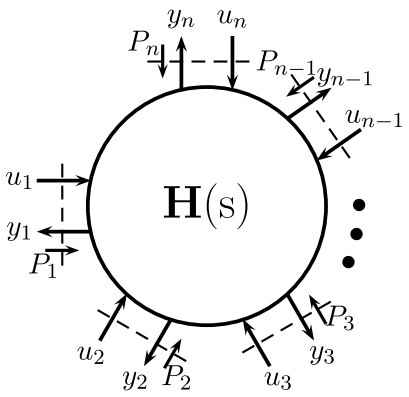


**Fig. 2.** A linear system $\mathbf{H}(s)$ characterized by $n$ energetic ports.

The total power flowing through the system is given by:

$$P_T = \sum_{i\in P_I} P_i + \sum_{j\in P_O} P_j = \sum_{i=1}^{n} u_i y_i = \mathbf{u}^{\mathrm{T}}\mathbf{y}. \tag{5}$$

**Definition 1.** System $\mathbf{H}_0$ is passive if $P_T = \mathbf{u}^{\mathrm{T}}\mathbf{y} > 0$, $\forall\, \mathbf{u} \neq 0$, that is if the total power $\sum_{i\in P_I} P_i$ entering the system is always larger than the total power $\sum_{j\in P_O} P_j$ exiting the system any time $\mathbf{u} \neq 0$.

**Property 1.** *Given an n-ports linear physical system, a necessary and sufficient condition for it to be passive is that the symmetric part of matrix* $\mathbf{H}_0$ *in (4) is positive definite:*

$$\mathbf{H}_{0_s} = \frac{\mathbf{H}_0 + \mathbf{H}_0^{\mathrm{T}}}{2} > 0. \tag{6}$$

**Proof.** Using (4), the total power flow $P_T = \mathbf{u}^{\mathrm{T}}\mathbf{y}$ in (5) becomes:

$$P_T = \mathbf{u}^{\mathrm{T}}\,\mathbf{H}_0\,\mathbf{u} > 0. \tag{7}$$

The total power flow $P_T$ in (7) is a quadratic function of matrix $\mathbf{H}_0$. It is well known that $P_T = \mathbf{u}^{\mathrm{T}}\mathbf{y} > 0$ is positive definite iff the symmetric part of the steady-state transfer matrix $\mathbf{H}_0$ is positive definite, that is if relation (6) holds. □

**Definition 2.** In steady-state condition, the efficiency $E(t)$ of an n-ports passive system having the structure shown in Fig. 2 is defined as follows:

$$E(t) = \frac{-\left(\sum_{j\in P_O} P_j\right)}{\sum_{i\in P_I} P_i}, \tag{8}$$

where sets $P_I$ and $P_O$ are defined in (1) and (2).

Note: the efficiency $E(t)$ in (8) is not defined when $\sum_{i\in P_I} P_i = 0$, as in this case the entering power is zero, which cannot happen since the system is supposed to be passive.

## 4. Two-ports linear system

This section is focused on the study of the two-ports linear systems class. Reference is made to the general case in Fig. 2 when the number of ports is $n = 2$. The steady-state description of the system given in (4) can be expanded as:

$$\underbrace{\begin{bmatrix} y_1 \\ y_2 \end{bmatrix}}_{\mathbf{y}} = \underbrace{\begin{bmatrix} a & b \\ -c & d \end{bmatrix}}_{\mathbf{H}_0} \underbrace{\begin{bmatrix} u_1 \\ u_2 \end{bmatrix}}_{\mathbf{u}}, \tag{9}$$

where $a$, $b$, $c$ and $d$ are the coefficients within matrix $\mathbf{H}_0$. The necessary and sufficient condition for the two-ports linear system (9) to be passive is given by inequality (6). Using the Sylvester's criterion, one can easily prove that matrix $\mathbf{H}_{0_s}$ is positive definite iff the following inequalities hold:

$$(a > 0) \wedge (d > 0) \wedge \left(ad > \frac{(b-c)^2}{4}\right). \tag{10}$$

**Property 2.** *If linear system* $\mathbf{H}(s)$ *is characterized by* $b = -c$, *then* $(a > 0) \wedge (d > 0) \wedge \left(\det(\mathbf{H}_0) = ad + bc > 0\right)$ *is a* necessary and sufficient condition *for the system to be passive. If linear system* $\mathbf{H}(s)$ *is characterized by* $b \neq -c$, *then* $(a > 0) \wedge (d > 0) \wedge \left(\det(\mathbf{H}_0) = ad + bc > 0\right)$ *is a* necessary but not sufficient condition *for the system to be passive.*

**Proof.** The proof is given in Appendix A.

Note: for the two-ports linear systems case, it is more intuitive to perform the study of the system efficiency by assuming that power $P_2 = u_2\, y_2$ is positive when exiting the system, thus ascribing to the sign notation which is adopted by the authors in [41,42]. This can be achieved by changing the sign of one of the two power variables characterizing power $P_2 = u_2\, y_2$, see [2]. By changing the sign of power variable $y_2$, the description in (9) turns into:

$$\underbrace{\begin{bmatrix} y_1 \\ -y_2 \end{bmatrix}}_{\mathbf{y}} = \underbrace{\begin{bmatrix} a & b \\ -c & d \end{bmatrix}}_{\mathbf{H}_0} \underbrace{\begin{bmatrix} u_1 \\ u_2 \end{bmatrix}}_{\mathbf{u}} \quad \Leftrightarrow \quad \underbrace{\begin{bmatrix} y_1 \\ y_2 \end{bmatrix}}_{\mathbf{y}} = \underbrace{\begin{bmatrix} a & b \\ c & -d \end{bmatrix}}_{\mathbf{H}_0} \underbrace{\begin{bmatrix} u_1 \\ u_2 \end{bmatrix}}_{\mathbf{u}}. \tag{11}$$

Since the two expressions in (11) are equivalent, reference will be made to (11) on the right. Let us refer to a real physical system case study allowing a bidirectional power flow, such as a PMSM (Permanent Magnet Synchronous Motor), see [41]-Section IV-C. The meaning of the new sign notation in (11) on the right is the following: the case $(P_1 > 0) \wedge (P_2 > 0)$ denotes the operation of the PMSM in *forward operating mode*, that is when the power is flowing from the electrical part (power $P_1 = u_1\, y_1$) to the mechanical part (power $P_2 = u_2\, y_2$) and the PMSM is working as a *motor* driving a certain load. Conversely, the case $(P_1 < 0) \wedge (P_2 < 0)$ denotes the operation of the PMSM in *reverse operating mode*, that is when the power is flowing from the mechanical part (power $P_2 = u_2\, y_2$) to the electrical part (power $P_1 = u_1\, y_1$) and the PMSM is working as a *generator* driven by some other source to generate electrical power.

**Definition 3.** In steady-state condition and by adopting the sign notation in (11) on the right, the efficiency $E(t)$ of a two-ports passive linear system is defined as follows:

$$E(t) = \begin{cases} \dfrac{u_2\, y_2}{u_1\, y_1} = E_f(t) & \text{if} \quad \left(P_1 > 0\right) \wedge \left(P_2 > 0\right), \\ \dfrac{u_1\, y_1}{u_2\, y_2} = \dfrac{1}{E_f(t)} & \text{if} \quad \left(P_1 < 0\right) \wedge \left(P_2 < 0\right), \\ 0 & \text{if} \quad \left(P_1 > 0\right) \wedge \left(P_2 < 0\right). \end{cases} \tag{12}$$

Function $E_f(t)$ represents the system efficiency in forward operating mode, whereas function $E_r(t) = 1/E_f(t)$ in (12) represents the system efficiency in reverse operating mode. The third case in (12) foresees both power flows entering the system and being fully dissipated inside it (i.e. no output power is present). The case of both powers exiting the system can never happen since the physical system is supposed to be passive, i.e. the parameters of matrix $\mathbf{H}_0$ must obey conditions (10).

The efficiency of a two-ports linear system can be studied both using the power variables $(y_2, u_2)$ of the second system energetic port and using the power variables $(y_1, u_1)$ of the first system energetic port. The two analyses are performed in Section 4.1 and in Section 4.2, respectively. One can verify that the static input–output description of the two-ports linear system in (11) can also be expressed as follows:

$$\begin{bmatrix} u_1 \\ y_1 \end{bmatrix} = \underbrace{\begin{bmatrix} \frac{d}{c} & \frac{1}{c} \\ \frac{ad+bc}{c} & \frac{a}{c} \end{bmatrix}}_{\mathbf{T}_{21}} \begin{bmatrix} u_2 \\ y_2 \end{bmatrix}, \qquad \begin{bmatrix} u_2 \\ y_2 \end{bmatrix} = \underbrace{\begin{bmatrix} -\frac{a}{b} & \frac{1}{b} \\ \frac{ad+bc}{b} & -\frac{d}{b} \end{bmatrix}}_{\mathbf{T}_{12}} \begin{bmatrix} u_1 \\ y_1 \end{bmatrix}. \tag{13}$$

By replacing (13) in the expression of $E_f(t)$ in (12), one obtains the following two equivalent representations of the system forward efficiency on planes $(y_2, u_2)$ and $(y_1, u_1)$:

$$E_f(y_2, u_2) = \frac{c^2\, u_2\, y_2}{(d\, u_2 + y_2)\,[(a\, d + b\, c)\, u_2 + a\, y_2]}, \tag{14}$$

$$E_f(y_1, u_1) = \frac{(-a\, u_1 + y_1)\,[(a\, d + b\, c)\, u_1 - d\, y_1]}{b^2\, u_1\, y_1}. \tag{15}$$

### 4.1. Analysis on plane $(y_2, u_2)$

**Property 3.** *Two-ports linear systems exhibit a constant efficiency* $E(t)$ *along straight lines exiting from the origin of plane* $(y_2, u_2)$*:*

$$u_2 = \gamma\, y_2, \qquad \gamma \in [-\infty,\ \infty]. \tag{16}$$

*The efficiency* $E(t)$ *reaches its maximum value* $E^*$ *in forward operating mode for* $\gamma = \gamma^*$*:*

$$E^* = \frac{c(\sqrt{ad + bc} - \sqrt{ad})}{b(\sqrt{ad + bc} + \sqrt{ad})}, \qquad \gamma^* = \sqrt{\frac{a}{d\,(a\, d + c\, b)}}, \tag{17}$$

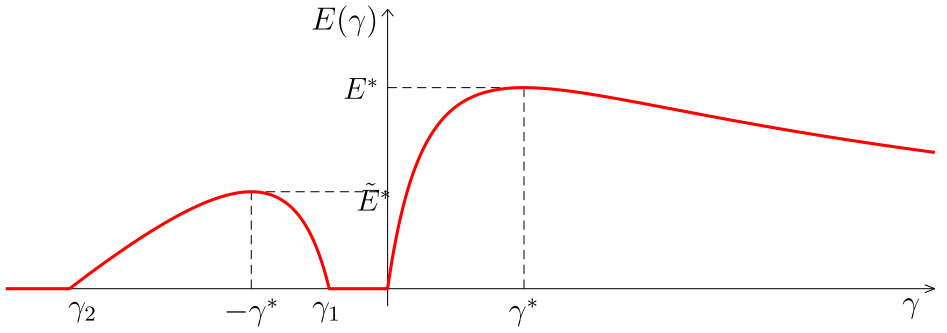


**Fig. 3.** Full system efficiency $E(\gamma)$ as a function of parameter $\gamma$.

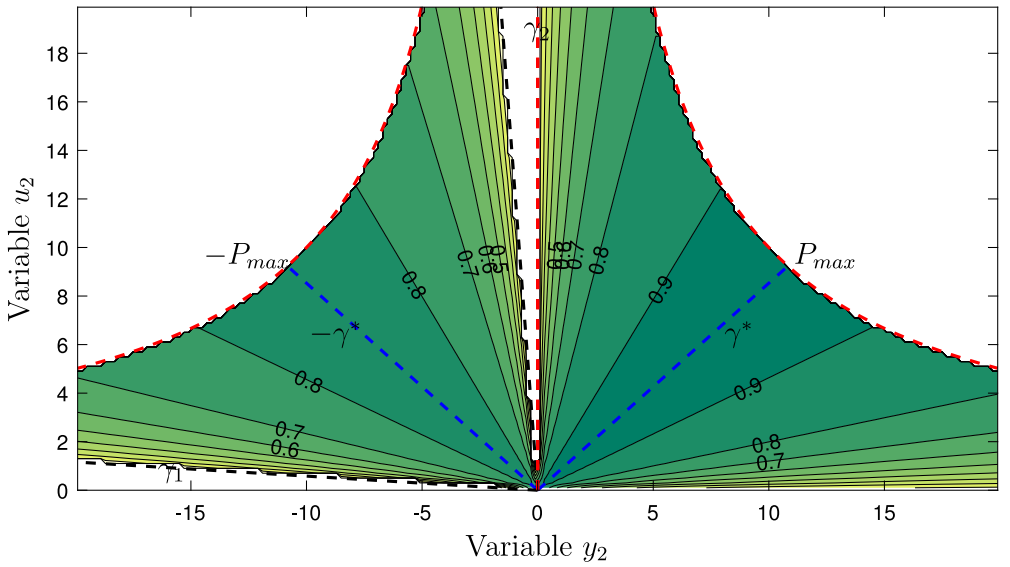


**Fig. 4.** Efficiency map $E$ shown on plane $(y_2, u_2)$.

*and its maximum value $\tilde{E}^*$ in reverse operating mode for $\gamma = -\gamma^*$:*

$$\tilde{E}^* = \frac{b(\sqrt{ad+bc} - \sqrt{ad})}{c(\sqrt{ad+bc} + \sqrt{ad})}, \qquad -\gamma^* = -\sqrt{\frac{a}{d\,(a\,d + c\,b)}}. \tag{18}$$

**Proof.** The proof is given in Appendix B.

The system efficiency $E(\gamma)$ vs. $\gamma$ shown in Fig. 3 has been obtained using the following parameters:

$$a = 0.05, \quad b = 0.9, \quad c = 0.95, \quad d = 0.08, \quad P_{max} = 100\,\text{W}. \tag{19}$$

Its equivalent representation $E(y_2, u_2)$, see (12) and (14), is shown in Fig. 4. The latter figure shows that the efficiency is indeed constant along straight lines exiting from the origin of plane $(y_2, u_2)$, in agreement with Property 3. Furthermore, the maximum forward and reverse efficiencies $E^*$ and $\tilde{E}^*$ do not coincide, i.e. the corresponding blue dashed lines $\gamma = \gamma^*$ and $\gamma = -\gamma^*$ in Fig. 4 fall within two contour regions having different color shades. This well agrees with what is stated in [42]-Property 2, since the system parameters *do not* satisfy $|b| = |c|$, see (19).

### 4.2. Analysis on plane $(y_1, u_1)$

**Property 4.** *Two-ports linear systems exhibit a constant efficiency $E(t)$ along straight lines exiting from the origin of plane $(y_1, u_1)$:*

$$u_1 = \alpha\, y_1, \qquad \alpha \in [-\infty,\ \infty]. \tag{20}$$

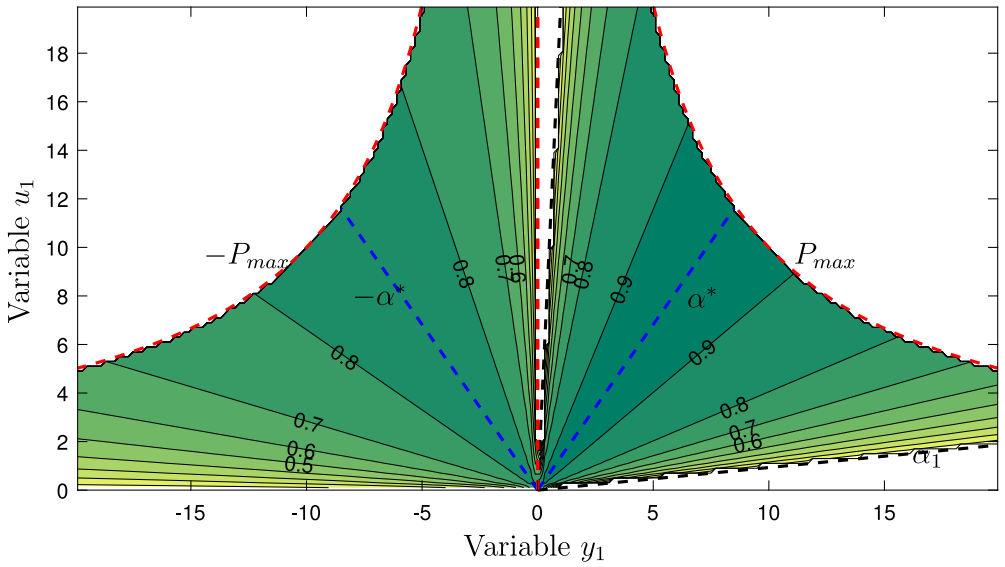


**Fig. 5.** Efficiency map $E$ shown on plane $(y_1, u_1)$.

*The efficiency $E(t)$ reaches its maximum value $E^*$ in forward operating mode for $\alpha = \alpha^*$:*

$$E^* = \frac{c(\sqrt{ad+bc} - \sqrt{ad})}{b(\sqrt{ad+bc} + \sqrt{ad})}, \qquad \alpha^* = \sqrt{\frac{d}{a(a\,d + b\,c)}},$$

*and its maximum value $\tilde{E}^*$ in reverse operating mode for $\alpha = -\alpha^*$:*

$$\tilde{E}^* = \frac{b(\sqrt{ad+bc} - \sqrt{ad})}{c(\sqrt{ad+bc} + \sqrt{ad})}, \qquad -\alpha^* = -\sqrt{\frac{d}{a(a\,d + b\,c)}}.$$

**Proof.** The proof is given in Appendix C.

The efficiency map $E(y_1, u_1)$ for a system characterized by the parameters in (19) is shown in Fig. 5. For the latter, the same considerations as those made for the efficiency map $E(y_2, u_2)$ in Fig. 4 hold, since the two representations are interchangeable through (13) and provide the same efficiency information shown on the two operating planes $(y_1, u_1)$ and $(y_2, u_2)$ given by the power variables of the first and second system energetic ports, respectively.

### 4.3. Design parameter for two-ports linear systems

Let us consider a two-ports linear system $\mathbf{H}(s)$ satisfying the condition $|b| = |c|$. According to [42]-Property 2, the considered system is going to exhibit the same maximum forward and reverse efficiency $E^* = \tilde{E}^*$, which can be written as:

$$E^*(q) = \frac{|\sqrt{1+q}-1|}{\sqrt{1+q}+1} = \begin{cases} E^*_+(q) & \text{if} \quad q > 0 \ (b = c), \\ E^*_-(q) & \text{if} \quad -1 \le q \le 0 \ (b = -c), \end{cases} \tag{21}$$

where:

$$E^*_+(q) = \frac{\sqrt{1+q}-1}{\sqrt{1+q}+1}, \qquad E^*_-(q) = -\frac{\sqrt{1+q}-1}{\sqrt{1+q}+1},$$

and parameter $q$ is defined as follows:

$$\boxed{q = \frac{b\,c}{a\,d}} \tag{22}$$

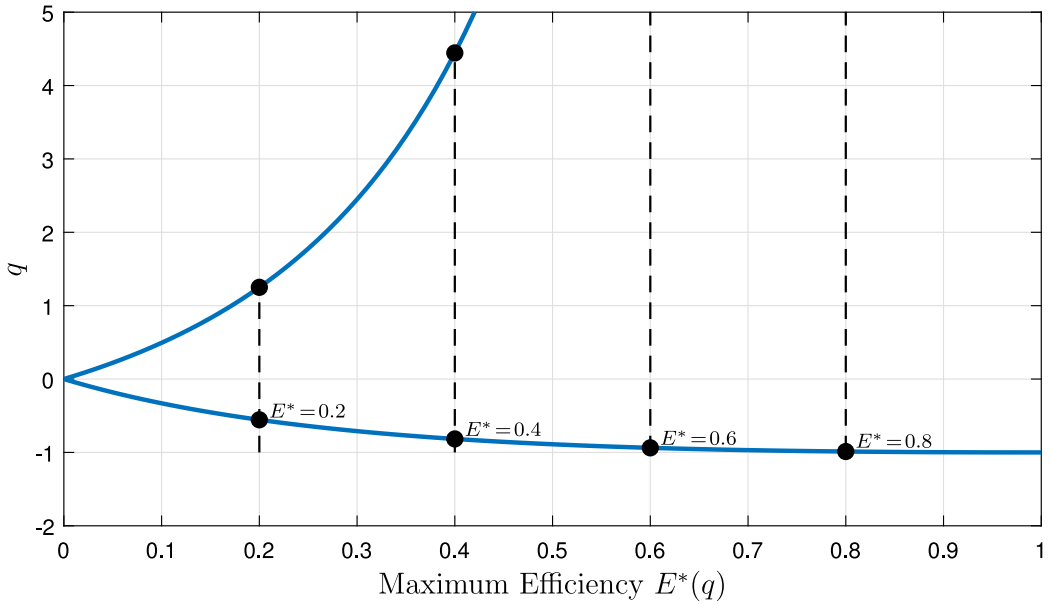


**Fig. 6.** Parameter $q$ as a function of the maximum efficiency $E^*(q)$.

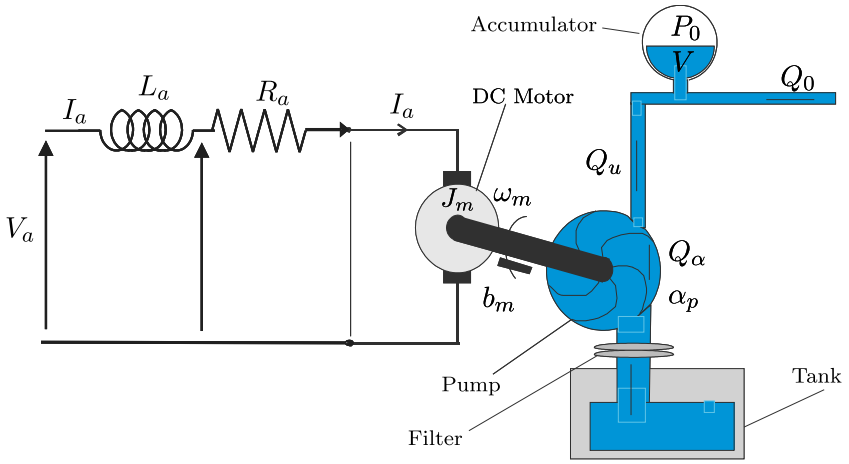


**Fig. 7.** A DC motor driving an hydraulic pump.

The global behavior of function $E^*(q)$ for $q \in [-1, +\infty)$ is shown in [42]-Fig. 12. One can easily prove that function $E^*(q)$ in (21) can be inverted as follows:

$$q(E^*) = \begin{cases} \left(\dfrac{E^* + 1}{1 - E^*}\right)^2 - 1 & \text{for} \quad q > 0, \\ \left(\dfrac{-E^* + 1}{1 + E^*}\right)^2 - 1 & \text{for} \quad -1 \le q \le 0. \end{cases} \tag{23}$$

The global behavior of function $q(E^*)$ for $E^* \in [0, 1]$ is shown in Fig. 6. From [42]-Fig. 12 and Fig. 6, it results that parameter $q$ in (22) can be exploited as a *design parameter* for two-ports linear systems. The designer may need to evaluate the maximum efficiency of the considered system; to do that, matrix $\mathbf{H}_0$ in (11) must be computed. Once the designer has discriminated whether condition $b = -c$ (i.e. $-1 \le q \le 0$) or $b = c$ (i.e. $q > 0$) holds, reference can be made to the left-hand side or to the right hand-side of the plot in [42]-Fig. 12, showing the maximum efficiency $E^*$ of the system (in both forward and reverse operating mode) as a function of parameter $q$ in (22). Alternatively, the designer may be given a certain specification in terms of maximum efficiency $E^*$ of the considered system. In this case, once the designer has computed matrix $\mathbf{H}_0$ in (11) and discriminated whether condition $b = -c$ (i.e. $-1 \le q \le 0$) or $b = c$ (i.e. $q > 0$) holds, reference can be made to the lower part or to the upper part of the plot in Fig. 6, in

order to determine the value of parameter $q$ that the system must exhibit so as to satisfy the specification in terms of maximum efficiency $E^*$.

### 4.4. Two-ports systems: case study

The considered case study is a DC electric motor driving an hydraulic pump, whose schematic representation is shown in Fig. 7.

#### 4.4.1. Linear case

In the linear case, this system has been modeled in [35], whereas its efficiency analysis is addressed in this section for the first time. The state space model of the system is:

$$\underbrace{\begin{bmatrix} L_a & 0 & 0 \\ 0 & J_m & 0 \\ 0 & 0 & C_0 \end{bmatrix}}_{\mathbf{L}} \underbrace{\begin{bmatrix} \dot{I}_a \\ \dot{\omega}_m \\ \dot{P}_0 \end{bmatrix}}_{\dot{\mathbf{x}}} = \underbrace{\begin{bmatrix} -R_a & -K_m & 0 \\ K_m & -b_m & -K_p \\ 0 & K_p & -\alpha_p \end{bmatrix}}_{\mathbf{A}} \underbrace{\begin{bmatrix} I_a \\ \omega_m \\ P_0 \end{bmatrix}}_{\mathbf{x}} + \underbrace{\begin{bmatrix} 1 & 0 \\ 0 & 0 \\ 0 & -1 \end{bmatrix}}_{\mathbf{B}} \underbrace{\begin{bmatrix} V_a \\ Q_0 \end{bmatrix}}_{\mathbf{u}},$$

$$\mathbf{y} = \underbrace{\begin{bmatrix} 1 & 0 & 0 \\ 0 & 0 & 1 \end{bmatrix}}_{\mathbf{C}} \mathbf{x}.$$

The reader is referred to [35] for details about the system parameters and variables. The elements of matrix $\mathbf{H}_0$ are:

$$a = \frac{K_p^2 + \alpha_p b_m}{\alpha_p K_m^2 + R_a K_p^2 + R_a \alpha_p b_m}, \qquad d = \frac{K_m^2 + R_a b_m}{\alpha_p K_m^2 + R_a K_p^2 + R_a \alpha_p b_m},$$
$$b = \frac{-K_m K_p}{\alpha_p K_m^2 + R_a K_p^2 + R_a \alpha_p b_m} = -c. \tag{24}$$

The considered system satisfies $|b| = |c|$, see [42]-Property 2, meaning that the maximum efficiency in forward and reverse operating modes coincide and are given by $E^* = \tilde{E}^* = E^*(q) = E^*_-(q)$ in (21) when $-1 \le q \le 0$ (as $b$ and $c$ have opposite sign), see the left-hand side of the plot in [42]-Fig. 12. The design parameter $q$ can be computed by replacing (24) in (22), see the expression of $q$ in (25). Furthermore, the expression of the slope $\gamma^*$ in (17) can be elaborated so as to express $\gamma^*$ as a function of parameter $q$, see the expression of $\gamma^*$ in (25).

$$q = -\frac{K_m^2 K_q^2}{(K_m^2 + R_a b_m)(K_p^2 + \alpha_p b_m)} < 0, \qquad \gamma^* = \left(\frac{1}{d}\right)\sqrt{\frac{1}{1+q}}. \tag{25}$$

From (25), the designer can evince that the modulus of parameter $q$ increases if the dissipative terms $R_a$, $b_m$ and $\alpha_p$ decrease.

#### 4.4.2. Nonlinear case

By adding some nonlinearities which are present in the actual system, the considered system falls in the category of linear systems $\mathbf{H}(s)$ with additional nonlinear friction terms, see [42]-Fig. 13. In the present case, the nonlinearities added on planes $(y_1, \tilde{u}_1) = (I_a, \tilde{V}_a)$ and $(y_2, \tilde{u}_2) = (P_0, \tilde{Q}_0)$ are the following:

$$\begin{aligned} \tilde{u}_1 &= \tilde{V}_a = f_1(y_1) = f_1(I_a) = R_{sq}\, I_a\, |I_a|, \\ \tilde{u}_2 &= \tilde{Q}_0 = f_2(y_2) = f_2(P_0) = \alpha_0 \sqrt{P_0}\, \mathrm{sgn}(P_0), \end{aligned} \tag{26}$$

which are symmetric with respect to the origin. The first equation in (26) describes the Joule losses affecting the DC motor, whereas the second equation in (26) describes a nonlinear resistance affecting the hydraulic accumulator $C_0$. Assuming that the system parameters values are: $K_m = 5\ [\mathrm{Nm/A}]$, $R_a = 0.05\ [\Omega]$, $b_m = 2 \cdot 10^{-4}\ [(\mathrm{Nm\ s})/\mathrm{rad}]$, $R_{sq} = 4 \cdot 10^{-3}\ \left[\mathrm{V/A^2}\right]$, $K_p = 9\ [\mathrm{Nm/Pa}]$, $\alpha_p = 1 \cdot 10^{-4}\ \left[\mathrm{m^3/(s\ Pa)}\right]$, $\alpha_0 = 0.01\ \left[\mathrm{m^3/(s\ \sqrt{Pa})}\right]$, Fig. 8 shows the resulting efficiency map on plane $(y_2, u_2) = (P_0, Q_0)$. The latter is given in the half-plane $(P_0, Q_0 > 0)$ as it is symmetric with respect to the origin, see [42]-Property 3, since the two nonlinearities $f_1(y_1) = f_1(I_a)$ and $f_2(y_2) = f_2(P_0)$ affecting the system are symmetric with respect to the origin of the corresponding planes $(y_1, \tilde{u}_1) = (I_a, \tilde{V}_a)$ and $(y_2, \tilde{u}_2) = (P_0, \tilde{Q}_0)$.

## 5. Three-ports linear system

This section is focused on the study of the three-ports linear system shown in Fig. 9, namely a single-stage planetary gear set. According to the notation adopted in Fig. 2 for a generic $n$-ports linear system, the power flows $P_r = T_r\, \omega_r$, $P_s = T_s\, \omega_s$ and $P_c = T_c\, \omega_c$ are positive if entering the ring, sun and carrier energetic ports, respectively. The rigid reduced-order state–space model of the single-stage planetary gear set can be derived by applying the systematic methodology described by the authors in [33]:

$$\begin{cases} \mathbf{L}\,\dot{\mathbf{x}} = \mathbf{A}\,\mathbf{x} + \mathbf{B}\,\mathbf{u} \\ \mathbf{y} = \mathbf{B}^{\mathrm{T}}\,\mathbf{x} \end{cases}, \qquad \mathbf{u} = \begin{bmatrix} T_c \\ T_s \\ T_r \end{bmatrix}, \qquad \mathbf{y} = \begin{bmatrix} \omega_c \\ \omega_s \\ \omega_r \end{bmatrix}, \qquad \mathbf{x} = \begin{bmatrix} \omega_c \\ \omega_r \end{bmatrix},$$
$$\mathbf{L} = \begin{bmatrix} J_{11} & J_{12} \\ J_{12} & J_{22} \end{bmatrix}, \qquad \mathbf{A} = \begin{bmatrix} a_{11} & a_{12} \\ a_{12} & a_{22} \end{bmatrix}, \qquad \mathbf{B} = \begin{bmatrix} 1 & b_{12} & 0 \\ 0 & b_{21} & 1 \end{bmatrix}, \tag{27}$$

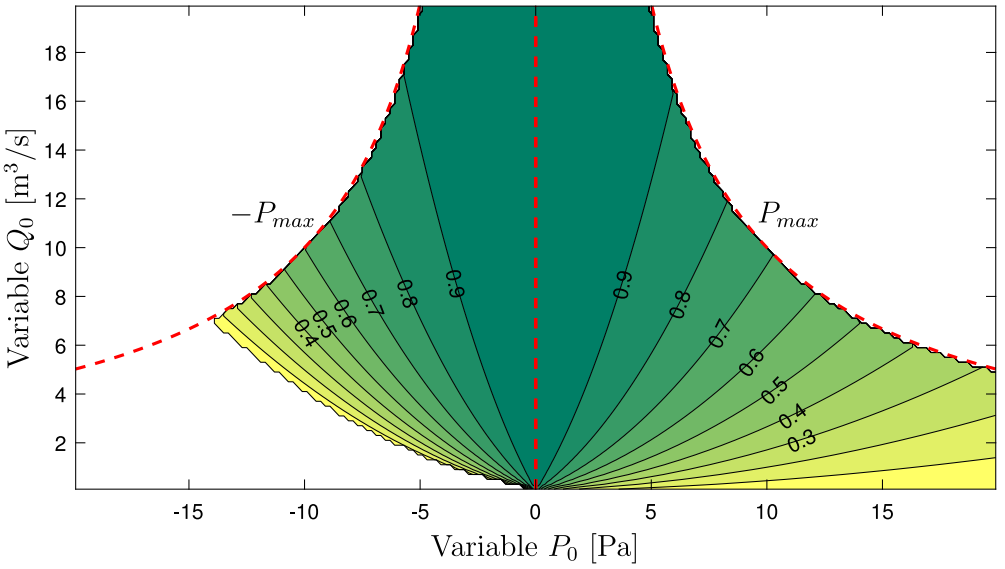


**Fig. 8.** Efficiency map $E(y_2, u_2) = E(P_0, Q_0)$ of the DC motor with hydraulic pump.

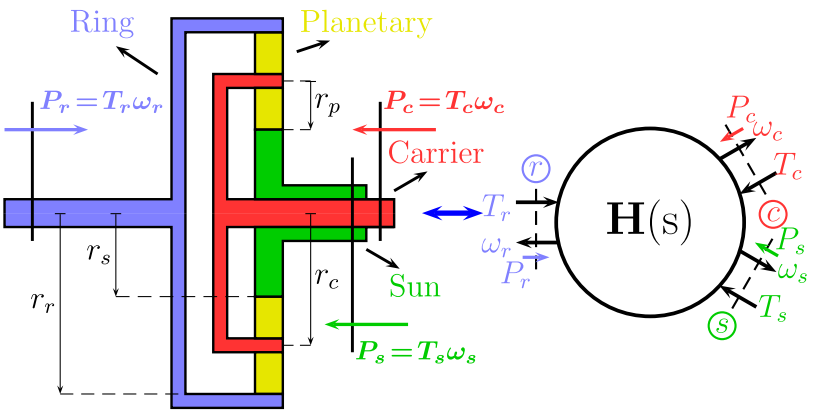


**Fig. 9.** Single-stage planetary gear set: structure and model.

where $b_{12} = 2r_c/r_{s1}$, $b_{21} = -r_r/r_{s1}$ and the elements of $\mathbf{L}$ and $\mathbf{A}$ can be computed using [33]-(7). The static input–output relation $\mathbf{y} = \mathbf{H}_0\,\mathbf{u}$ of system (27), see (4), is characterized by matrix $\mathbf{H}_0 \in \mathcal{R}^{(3\times3)}$ having rank equal to 2:

$$\mathbf{H}_0 = -\mathbf{B}^{\mathrm{T}}\mathbf{A}^{-1}\mathbf{B} = -\begin{bmatrix} 1 & 0 \\ b_{12} & b_{21} \\ 0 & 1 \end{bmatrix}\begin{bmatrix} a_{11} & a_{12} \\ a_{12} & a_{22} \end{bmatrix}^{-1}\begin{bmatrix} 1 & b_{12} & 0 \\ 0 & b_{21} & 1 \end{bmatrix}. \tag{28}$$

**Property 5.** *In steady-state condition, the single-stage planetary gear set behaves as a degenerate three-ports system, since the components $\omega_c$, $\omega_s$, $\omega_r$ of the output vector $\mathbf{y}$ and the components $T_c$, $T_s$, $T_r$ of the minimum norm input vector $\mathbf{u}$ are constrained as follows:*

$$\omega_s = b_{12}\,\omega_c + b_{21}\,\omega_r, \qquad T_s = b_{12}T_c + b_{21}T_r. \tag{29}$$

**Proof.** The proof of the algebraic relations (29) is given in Appendix D, see (D.1) and (D.4).

Using $\mathbf{y} = \mathbf{H}_0\mathbf{u}$, (28) and (29), one can easily verify that the static relation $\mathbf{y}_r = \mathbf{H}_{0_r}\mathbf{u}_r$ between the reduced vectors $\mathbf{y}_r$ and $\mathbf{u}_r$ can be obtained:

$$\underbrace{\begin{bmatrix} \omega_c \\ \omega_r \end{bmatrix}}_{\mathbf{y}_r} = \mathbf{H}_{0_r}\underbrace{\begin{bmatrix} T_c \\ T_r \end{bmatrix}}_{\mathbf{u}_r}, \qquad \text{where} \qquad \mathbf{H}_{0_r} = -\mathbf{A}^{-1}\mathbf{B}\mathbf{B}^{\mathrm{T}} \tag{30}$$

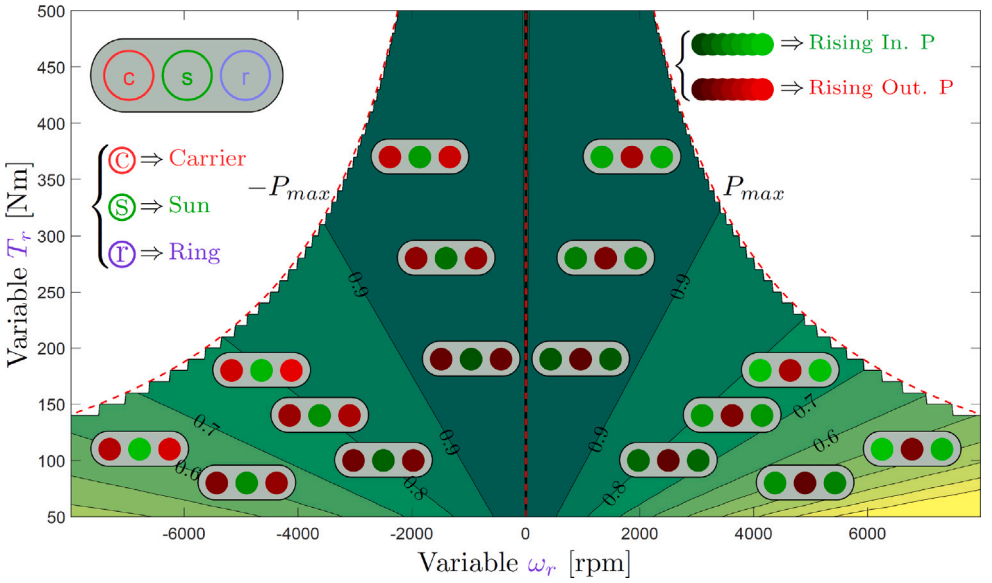


**Fig. 10.** Efficiency map $E$ of the single-stage planetary gear set shown on plane $(\omega_r, T_r)$.

**Table 1**
Parameters of the single-stage planetary gear set in Fig. 9.

| | | | |
|---|---|---|---|
| $r_c = 0.228$ [m] | $r_p = 0.1$ [m] | $r_s = 0.128$ [m] | $r_r = 0.328$ [m] |
| $b_c = 0.0764 \left[\frac{\text{Nm s}}{\text{rad}}\right]$ | $b_p = 305.58 \left[\frac{\text{Nm s}}{\text{rad}}\right]$ | $b_s = 0.002\, b_c$ | $b_r = 0.002\, b_c$ |

is a second order full rank matrix. Relation (30) can then be inverted as described in Section 4, see (13), in order to express the power variables of the carrier port as a function of the power variables of the ring port:

$$\begin{bmatrix} T_c \\ \omega_c \end{bmatrix} = \mathbf{T}_{rc} \begin{bmatrix} T_r \\ \omega_r \end{bmatrix}. \tag{31}$$

Using (29) and (31), in steady-state condition one can express the power variables $T_s$, $\omega_s$, $T_c$ and $\omega_c$ of the sun and carrier ports as a function of the power variables $T_r$, $\omega_r$ of the ring port. By applying the definition of efficiency in (8), one can finally build the single-stage planetary gear efficiency map $E(\omega_r, T_r)$ on the ring energetic port $(\omega_r, T_r)$. With a similar procedure, one can equivalently derive the efficiency maps $E(\omega_c, T_c)$ and $E(\omega_s, T_s)$ on the carrier and sun energetic ports. The efficiency map $E(\omega_r, T_r)$ of the single-stage planetary gear set when the system parameters take on the values reported in Table 1 is reported in Fig. 10. This figure shows that the system efficiency is constant along straight lines exiting from the origin of plane $(\omega_r, T_r)$, as the system is linear. Furthermore, in Fig. 10, a traffic light notation has been added to the efficiency map to describe the orientation and the magnitude of powers $P_c$, $P_s$ and $P_r$ flowing through the three system power sections. The circles within each traffic light are associated, from left to right, to the carrier, sun and ring system ports. If the considered circle is painted red, the corresponding power flow is *negative*, thus *exiting* the system. If the considered circle is painted green, the corresponding power flow is *positive*, thus *entering* the system. Furthermore, the lighter is the color shade of the considered circle, the higher is the magnitude of the corresponding power flow, and viceversa.

*Remarks:* (1) In the right-half plane $(\omega_r > 0, T_r)$ of the efficiency map $E(\omega_r, T_r)$ in Fig. 10, i.e. when power flow $P_r = T_r\, \omega_r > 0$ is entering the system, the carrier power flow $P_c = T_c\, \omega_c > 0$ is entering the system and the sun power flow $P_s = T_s\, \omega_s < 0$ is exiting the system. (2) In the left-half plane $(\omega_r < 0, T_r)$ of the efficiency map $E(\omega_r, T_r)$, i.e. when power flow $P_r = \omega_r\, T_r < 0$ is exiting the system, the carrier and sun power flows $P_c$ and $P_s$ are exiting and entering the system, respectively.

## 6. Four-ports linear system

This section is focused on the study of the four-ports linear system shown in Fig. 11, namely a Ravigneaux planetary gear set [34]. According to the notation adopted in Fig. 2 for a generic $n$-ports linear system, the power flows $P_t = T_t\, \omega_t$, $P_s = T_s\, \omega_s$, $P_c = T_c\, \omega_c$ and $P_r = T_r\, \omega_r$ are positive if entering the large sun, small sun, carrier and ring energetic ports, respectively. The rigid reduced-order state–space model of the Ravigneaux planetary gear set can be derived by applying the systematic methodology described by the

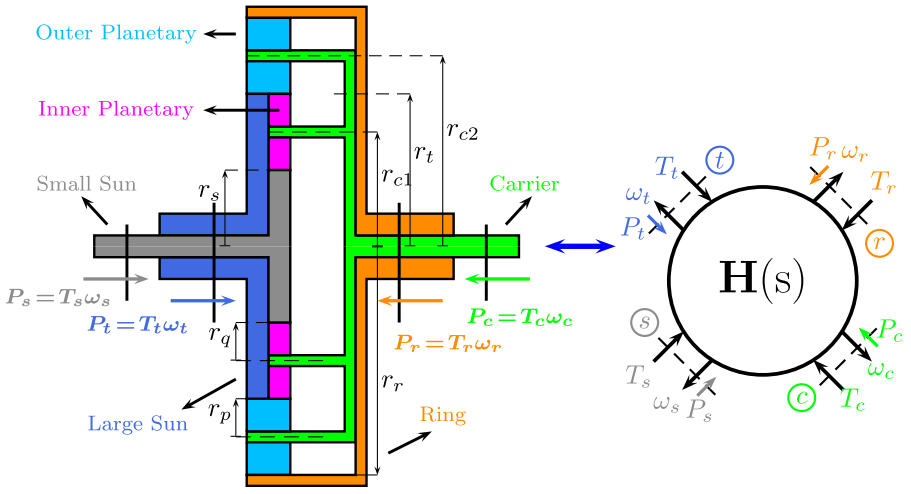


**Fig. 11.** Ravigneaux planetary gear set: structure and model.

authors in [34]:

$$\begin{cases} \mathbf{L}\,\dot{\mathbf{x}} = \mathbf{A}\,\mathbf{x} + \mathbf{B}\,\mathbf{u} \\ \mathbf{y} = \mathbf{B}^{\mathrm{T}}\,\mathbf{x} \end{cases}, \qquad \mathbf{u} = \begin{bmatrix} T_c \\ T_t \\ T_s \\ T_r \end{bmatrix}, \qquad \mathbf{y} = \begin{bmatrix} \omega_c \\ \omega_t \\ \omega_s \\ \omega_r \end{bmatrix}, \qquad \mathbf{x} = \begin{bmatrix} \omega_c \\ \omega_r \end{bmatrix},$$
$$\mathbf{L} = \begin{bmatrix} J_{11} & J_{12} \\ J_{12} & J_{22} \end{bmatrix}, \qquad \mathbf{A} = \begin{bmatrix} a_{11} & a_{12} \\ a_{12} & a_{22} \end{bmatrix}, \qquad \mathbf{B} = \begin{bmatrix} 1 & b_{12} & b_{13} & 0 \\ 0 & b_{21} & b_{23} & 1 \end{bmatrix}, \tag{32}$$

where $b_{12} = 2\,r_{c2}/r_t$, $b_{13} = 2\,(r_{c1} - r_{c2})/r_s$, $b_{21} = -r_r/r_t$ and $b_{23} = r_r/r_s$. The elements of $\mathbf{L}$ and $\mathbf{A}$ can be computed using [34]-(23). The static input–output relation $\mathbf{y} = \overline{\mathbf{H}}_0\,\mathbf{u}$ of system (32), see (4), is characterized by the following matrix $\overline{\mathbf{H}}_0 \in \mathcal{R}^{(4\times4)}$ having rank equal to 2:

$$\overline{\mathbf{H}}_0 = -\mathbf{B}^{\mathrm{T}}\mathbf{A}^{-1}\mathbf{B} = -\begin{bmatrix} 1 & 0 \\ b_{12} & b_{21} \\ b_{13} & b_{23} \\ 0 & 1 \end{bmatrix} \begin{bmatrix} a_{11} & a_{12} \\ a_{12} & a_{22} \end{bmatrix}^{-1} \begin{bmatrix} 1 & b_{12} & b_{13} & 0 \\ 0 & b_{21} & b_{23} & 1 \end{bmatrix}. \tag{33}$$

**Property 6.** *In steady-state condition, the Ravigneaux planetary gear set behaves as a degenerate three-ports system, since the components $\omega_c$, $\omega_t$, $\omega_s$, $\omega_r$ of the output vector $\mathbf{y}$ and the components $T_c$, $T_t$, $T_s$, $T_r$ of the minimum norm input vector $\mathbf{u}$ are constrained as follows:*

$$\begin{bmatrix} \omega_t \\ \omega_s \end{bmatrix} = \begin{bmatrix} b_{12} & b_{21} \\ b_{13} & b_{23} \end{bmatrix} \underbrace{\begin{bmatrix} \omega_s \\ \omega_r \end{bmatrix}}_{\mathbf{y}_r}, \qquad \begin{bmatrix} T_t \\ T_s \end{bmatrix} = \begin{bmatrix} b_{12} & b_{21} \\ b_{13} & b_{23} \end{bmatrix} \underbrace{\begin{bmatrix} T_s \\ T_r \end{bmatrix}}_{\mathbf{u}_r}. \tag{34}$$

**Proof.** The proof of the algebraic relations (34) is given in Appendix E, see (E.1) and (E.2).

Using $\mathbf{y} = \overline{\mathbf{H}}_0\mathbf{u}$, (33) and (34), one can easily verify that the static relation $\mathbf{y}_r = \overline{\mathbf{H}}_{0_r}\mathbf{u}_r$ between the reduced vectors $\mathbf{y}_r$ and $\mathbf{u}_r$ can be obtained:

$$\underbrace{\begin{bmatrix} \omega_c \\ \omega_r \end{bmatrix}}_{\mathbf{y}_r} = \overline{\mathbf{H}}_{0_r} \underbrace{\begin{bmatrix} T_c \\ T_r \end{bmatrix}}_{\mathbf{u}_r}, \tag{35}$$

where $\overline{\mathbf{H}}_{0_r} = -\mathbf{A}^{-1}\mathbf{B}\mathbf{B}^{\mathrm{T}}$ is a second order full rank matrix. Relation (35) can then be inverted as described in Section 4, see (13), in order to express the power variables of the carrier port as a function of the power variables of the ring port:

$$\begin{bmatrix} T_c \\ \omega_c \end{bmatrix} = \overline{\mathbf{T}}_{rc} \begin{bmatrix} T_r \\ \omega_r \end{bmatrix}. \tag{36}$$

Using (34) and (36), in steady-state condition one can express the power variables $T_t$, $\omega_t$, $T_s$, $\omega_s$, $T_c$ and $\omega_c$ of the large sun, small sun and carrier ports as a function of the power variables $T_r$, $\omega_r$ of the ring port. By applying the definition of efficiency in (8),

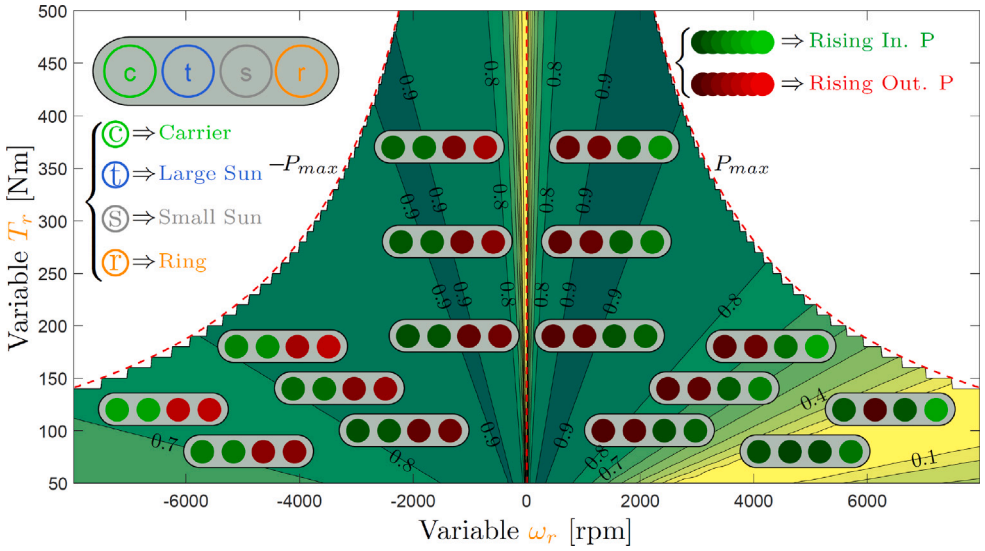


**Fig. 12.** Efficiency map $E$ of the Ravigneaux planetary gear set shown on plane $(\omega_r, T_r)$.

**Table 2**
Parameters of the Ravigneaux planetary gear set in Fig. 11.

| | | |
|---|---|---|
| $r_{c1} = 0.0875$ [m], $r_{c2} = 0.1575$ [m] | $r_p = 0.0525$ [m] | $r_q = 0.0175$ [m] |
| $r_t = 0.1050$ [m] | $r_s = 0.07$ [m] | $r_r = 0.21$ [m] |
| $b_c = b_p = b_q = b_t = b_s = b_r = 0.0955 \left[\frac{\text{Nm s}}{\text{rad}}\right]$, | $b_{st} = b_{cr} = b_{cq} = b_{cp} = 9.5493 \left[\frac{\text{Nm s}}{\text{rad}}\right]$ | |

one can finally build the efficiency map of the Ravigneaux planetary gear set $E(\omega_r, T_r)$ on the ring energetic port $(\omega_r, T_r)$. With a similar procedure, one can equivalently derive the efficiency maps $E(\omega_t, T_t)$, $E(\omega_s, T_s)$ and $E(\omega_c, T_c)$ on the large sun, small sun and carrier energetic ports. The efficiency map $E(\omega_r, T_r)$ of the Ravigneaux planetary gear set when the system parameters take on the values reported in Table 2 is reported in Fig. 12. In Fig. 12, a traffic light notation has been added to the efficiency map to describe the orientation and the magnitude of powers $P_c$, $P_t$, $P_s$ and $P_r$ flowing through the four system power sections. The circles within each traffic light are associated, from left to right, to the carrier, large sun, small sun and ring system ports. If the considered circle is painted red, the corresponding power flow is *negative*, thus *exiting* the system. If the considered circle is painted green, the corresponding power flow is *positive*, thus *entering* the system. Furthermore, the lighter is the color shade of the considered circle, the higher is the magnitude of the corresponding power flow, and viceversa.

*Remarks:* (1) In the right-half plane $(\omega_r > 0, T_r)$ of the efficiency map $E(\omega_r, T_r)$ in Fig. 12, i.e. when power flow $P_r = T_r \omega_r > 0$ is entering the system, the small sun power flow $P_s = T_s \omega_s > 0$ is entering the system. (2) In the left-half plane $(\omega_r < 0, T_r)$ of the efficiency map $E(\omega_r, T_r)$, i.e. when power flow $P_r = \omega_r T_r < 0$ is exiting the system, the carrier and the large sun power flows $P_c$ and $P_t$ are entering the system, whereas the small sun power flow $P_s$ is exiting the system.

## 7. Conclusion

In this paper, the formulation of the concepts of power efficiency and efficiency map for $n$-ports physical systems is addressed. The analysis is deepened for two-ports linear systems with mathematical proofs of the properties and showing the presence of a design parameter describing the system maximum efficiency. Three case studies are presented: a DC motor driving an hydraulic pump for the class of two-ports systems affected by nonlinearities, a single-stage planetary gear set for the class of three-ports linear systems, and a Ravigneaux planetary gear set for the class of four-ports linear systems. An important degree of freedom is given by the fact that the designer can choose the most suitable energetic port upon which the efficiency map is to be computed. This degree of freedom can be used by the designer to obtain the overall efficiency map of a complex system on the basis of the efficiency maps of its composing subsystems. The efficiency analysis presented in this paper has been performed with reference to the most generic case of $n$-ports physical systems, with the specific objective of providing the reader with all the tools for applying the proposed efficiency analysis to any physical system of their interest, in order to directly find the system efficiency maps. The proposed approach can therefore be useful for industries and engineers working with physical systems in different energetic domains, since the energy efficiency evaluation is becoming a more and more important topic nowadays.

## Declaration of competing interest

The authors declare that they have no known competing financial interests or personal relationships that could have appeared to influence the work reported in this paper.

## Funding

This research did not receive any specific grant from funding agencies in the public, commercial, or not-for-profit sectors.

## Appendix A

From (10), the following inequality holds:

$$\det \mathbf{H}_0 = ad + bc > \frac{(b-c)^2}{4} + bc = \frac{(b+c)^2}{4} \geq 0. \tag{A.1}$$

The following two cases are considered.

(a) $b = -c$. In this case, from (A.1) it follows that:

$$\det \mathbf{H}_0 = ad + bc \geq 0,$$

namely $(a > 0) \wedge (d > 0) \wedge (ad + bc > 0)$ is a *necessary and sufficient* condition for the system to be passive.

(b) $b \neq -c$. In this case, from (A.1) it follows that:

$$\det \mathbf{H}_0 = ad + bc > k = \frac{(b+c)^2}{4} > 0,$$

namely $(a > 0) \wedge (d > 0) \wedge (ad + bc > 0)$ is a *necessary but not sufficient* condition for the system to be passive.

## Appendix B

Substituting (16) in (14), the two-dimensional forward efficiency $E_f(y_2, u_2)$ turns into a one-dimensional representation:

$$E_f(\gamma) = \frac{c^2 \gamma}{(d\,\gamma + 1)\,[(a\,d + b\,c)\,\gamma + a]}. \tag{B.1}$$

Efficiency $E_f(\gamma)$ in (B.1) can also be written as:

$$E_f(\gamma) = \frac{c^2 \gamma}{a + \beta\,\gamma + \delta\,\gamma^2} \quad \text{where} \quad \begin{cases} \beta = 2\,a\,d + c\,b \\ \delta = d\,(a\,d + c\,b) \end{cases}. \tag{B.2}$$

The global behavior of efficiency $E_f(\gamma)$ in (B.2) as a function of parameter $\gamma$ is shown in [42]-Fig. 3. According to Property 2, condition $ad + bc > 0$ is a necessary condition for the system to be passive, from which one can evince that parameters $\beta$ and $\delta$ in (B.2) are both strictly greater than zero. Since $a > 0$ is another necessary condition for the system to be passive, according to the Routh's criterion it is possible to state that the two zeros $\gamma = \gamma_1$ and $\gamma = \gamma_2$ of the denominator of function $E(\gamma)$ in (B.2) have negative real part. Additionally, since the discriminant $\Delta = \beta^2 - 4a\delta = b^2c^2$ of equation $a + \beta\,\gamma + \delta\,\gamma^2 = 0$ is strictly greater than zero, the two solutions are real:

$$\gamma_1 = -\frac{a}{(a\,d + c\,b)}, \qquad \gamma_2 = -\frac{1}{d}. \tag{B.3}$$

The two zeros $\gamma = \gamma_1$ and $\gamma = \gamma_2$ represent the position of the two asymptotes of the function $E_f(\gamma)$, see [42]-Fig. 3. Deriving $E_f(\gamma)$ with respect to $\gamma$, one obtains:

$$\frac{\partial E_f(\gamma)}{\partial \gamma} = \frac{c^2(a - \delta\,\gamma^2)}{(a + \beta\,\gamma + \delta\,\gamma^2)^2}.$$

By solving $\frac{\partial E_f(\gamma)}{\partial \gamma} = 0$, one obtains the two solutions $\gamma^*$ and $-\gamma^*$ in (17) and (18) on the right. By computing $\frac{\partial^2 E_f(\gamma)}{\partial \gamma^2}$ and evaluating it for $\gamma = \pm\gamma^*$, one obtains:

$$\frac{\partial^2 E_f(\gamma)}{\partial \gamma^2} = \frac{-2c^2(a\beta + 3a\delta\gamma - \delta^2\gamma^3)}{(a + \beta\,\gamma + \delta\,\gamma^2)^3},$$

$$\frac{\partial^2 E_f(\gamma)}{\partial \gamma^2}\Big|_{\gamma=\gamma^*} < 0, \qquad \text{and} \qquad \frac{\partial^2 E_f(\gamma)}{\partial \gamma^2}\Big|_{\gamma=-\gamma^*} > 0,$$

from which it follows that $E_f(\gamma^*) = E_f^*$ is a local maximum of function $E_f(\gamma)$, whereas $E_f(-\gamma^*) = \bar{E}_f^*$ is a local minimum of function $E_f(\gamma)$, see [42]-Fig. 3. Replacing $\gamma = \gamma^*$ and $\gamma = -\gamma^*$ in function $E_f(\gamma)$ in (B.2), one obtains the expressions of the local maximum and minimum $E_f^*$ and $\bar{E}_f^*$:

$$E_f^* = \frac{c(\sqrt{ad + bc} - \sqrt{ad})}{b(\sqrt{ad + bc} + \sqrt{ad})}, \qquad \bar{E}_f^* = \frac{c(\sqrt{ad + bc} + \sqrt{ad})}{b(\sqrt{ad + bc} - \sqrt{ad})}. \tag{B.4}$$

According to the definition given in (12), function $E_f(\gamma)$ captures the one-dimensional representation of the two-ports system efficiency only when the power flow is oriented from the first system energetic port $(y_1, u_1)$ to the second system energetic port $(y_2, u_2)$, i.e. in forward operating mode. In fact, for $\gamma_2 < \gamma < \gamma_1$, function $E_f(\gamma)$ in (B.2) becomes greater than one (see [42]-Fig. 3), meaning that the power flow is actually reversed, i.e. oriented from the second system energetic port $(y_2, u_2)$ to the first system energetic port $(y_1, u_1)$, and the system is in reverse operating mode. For $\gamma \in (-\infty, \gamma_2) \cup (\gamma_1, 0)$, function $E_f(\gamma)$ in (B.2) becomes lower than zero (see [42]-Fig. 3), meaning that both power flows in the first and second system energetic ports $(y_1, u_1)$ and $(y_2, u_2)$ are entering the system, therefore the system efficiency is equal to zero according to the last condition in (12). From (12), it is evident that the system efficiency $E(t) = E(\gamma)$ can be expressed as a function of slope $\gamma$ relating the two power variables of plane $(y_2, u_2)$, see Fig. 3. The local maximum $E_f^*$ in (B.4) of the forward efficiency function $E_f(\gamma)$ becomes the absolute maximum $E^*$ of the full efficiency function $E(\gamma)$ when the system is in forward operating mode, i.e. for $\gamma > 0$ (see Fig. 3). Similarly, the inverse of the local minimum $\bar{E}_f^*$ in (B.4) of the forward efficiency function $E_f(\gamma)$ when $\gamma = -\gamma^*$ becomes the absolute maximum $\tilde{E}^* = 1/\bar{E}_f^*$ of the full efficiency function $E(\gamma)$ when the system is in reverse operating mode, i.e. for $\gamma_2 < \gamma < \gamma_1$ (see Fig. 3).

## Appendix C

Substituting (20) in (15), the two-dimensional forward efficiency $E_f(y_1, u_1)$ turns into a one-dimensional representation:

$$E_f(\alpha) = \frac{-d + \beta\,\alpha - \eta\,\alpha^2}{b^2\alpha} \qquad \text{where} \qquad \begin{cases} \beta = 2\,a\,d + c\,b \\ \eta = a(a\,d + b\,c) \end{cases}. \tag{C.1}$$

The global behavior of $E_f(\alpha)$ in (C.1) as a function of $\alpha$ is shown in [42]-Fig. 6. Following a procedure similar to that of Appendix B, it is possible to show that the two zeros of the numerator of function $E(\alpha)$ in (C.1) are real and positive: $\alpha_1 = d/(a\,d + c\,b)$ and $\alpha_2 = 1/a$. By solving $\frac{\partial E(\alpha)}{\partial \alpha} = 0$, one obtains the two solutions $\alpha^*$ and $-\alpha^*$ given in Property 4. It can be shown that $E_f(\alpha^*) = E_f^*$ is a local maximum of function $E_f(\alpha)$, whereas $E_f(-\alpha^*) = \bar{E}_f^*$ is a local minimum of function $E_f(\alpha)$. By computing the respective expressions, one can verify that they coincide with those reported in (B.4), as expected. According to (12), function $E_f(\alpha)$ captures the one-dimensional representation of the system efficiency in forward operating mode. By making similar considerations to those made in Appendix B for the analysis on plane $(y_2, u_2)$, the global behavior of the efficiency function $E(\alpha)$ can be determined, see [42]-Fig. 10. The local maximum $E_f^*$ in (B.4) of the forward efficiency function $E_f(\alpha)$ becomes the absolute maximum $E^*$ of the full efficiency function $E(\alpha)$ when the system is in forward operating mode, i.e. for $\alpha_1 < \alpha < \alpha_2$ (see [42]-Fig. 10). Similarly, the inverse of the local minimum $\bar{E}_f^*$ in (B.4) of the forward efficiency function $E_f(\alpha)$ becomes the absolute maximum $\tilde{E}^* = 1/\bar{E}_f^*$ of the full efficiency function $E(\alpha)$ when the system is in reverse operating mode, i.e. for $\alpha < 0$ (see [42]-Fig. 10).

## Appendix D

The algebraic constraint among the components of the output vector $\mathbf{y}$, i.e. the angular speeds $\omega_c$, $\omega_s$ and $\omega_r$, is given by the second equation $\mathbf{y} = \mathbf{B}^{\mathrm{T}}\mathbf{x} = \mathbf{B}^{\mathrm{T}}\mathbf{y}_r$ of system (27):

$$\underbrace{\begin{bmatrix} \omega_c \\ \omega_s \\ \omega_r \end{bmatrix}}_{\mathbf{y}} = \underbrace{\begin{bmatrix} 1 & 0 \\ b_{12} & b_{21} \\ 0 & 1 \end{bmatrix}}_{\mathbf{B}^{\mathrm{T}}} \underbrace{\begin{bmatrix} \omega_c \\ \omega_r \end{bmatrix}}_{\mathbf{x}=\mathbf{y}_r} \qquad \Rightarrow \qquad \omega_s = b_{12}\,\omega_c + b_{21}\,\omega_r. \tag{D.1}$$

In steady-state condition, i.e. when $\dot{\mathbf{x}} = 0$, the static input–output relation of system (27) is $\mathbf{y} = \mathbf{H}_0\mathbf{u}$ where $\mathbf{H}_0 = -\mathbf{B}^{\mathrm{T}}\mathbf{A}^{-1}\mathbf{B} \in \mathcal{R}^{(3\times3)}$, see (28). Since the rank of matrix $\mathbf{H}_0$ is 2, relation $\mathbf{y} = \mathbf{H}_0\mathbf{u}$ has solutions only if $\mathbf{y} \in \mathrm{Im}(\mathbf{B}^{\mathrm{T}})$. The set $\tilde{\mathbf{u}}$ of all the solutions $\mathbf{u}$ of relation $\mathbf{y} = \mathbf{H}_0\mathbf{u}$ when $\mathbf{y} \in \mathrm{Im}(\mathbf{B}^{\mathrm{T}})$ can be expressed as follows:

$$\tilde{\mathbf{u}} = \mathbf{u}_0 + \ker(\mathbf{B}), \tag{D.2}$$

where $\mathbf{u}_0$ is a particular solution and $\ker(\mathbf{B})$ is the kernel of matrix $\mathbf{B}$. The minimum norm solution $\mathbf{u}$ of set $\tilde{\mathbf{u}}$ in (D.2) is the one orthogonal to $\ker(\mathbf{B})$:

$$\mathbf{u} \in \ker(\mathbf{B})^{\perp} \qquad \Leftrightarrow \qquad \mathbf{u} \in \mathrm{Im}(\mathbf{B}^{\mathrm{T}}). \tag{D.3}$$

From (D.3), it follows that the minimum norm solution $\mathbf{u}$ can be expressed as follows as a function of the reduced vector $\mathbf{u}_r$:

$$\underbrace{\begin{bmatrix} T_c \\ T_s \\ T_r \end{bmatrix}}_{\mathbf{u}} = \underbrace{\begin{bmatrix} 1 & 0 \\ b_{12} & b_{21} \\ 0 & 1 \end{bmatrix}}_{\mathbf{B}^{\mathrm{T}}} \underbrace{\begin{bmatrix} T_c \\ T_r \end{bmatrix}}_{\mathbf{u}_r} \qquad \Rightarrow \qquad T_s = b_{12}\,T_c + b_{21}\,T_r. \tag{D.4}$$

Relation (D.4) is an algebraic constraint between the components $T_c$, $T_s$ and $T_r$ of the input vector $\mathbf{u}$.

## Appendix E

The algebraic constraint among the components of the output vector $\mathbf{y}$, i.e. the angular speeds $\omega_c$, $\omega_t$, $\omega_s$ and $\omega_r$, is given by the second equation $\mathbf{y} = \mathbf{B}^{\mathrm{T}}\mathbf{x} = \mathbf{B}^{\mathrm{T}}\mathbf{y}_r$ of system (32):

$$\underbrace{\begin{bmatrix}\omega_c\\ \omega_t\\ \omega_s\\ \omega_r\end{bmatrix}}_{\mathbf{y}} = \underbrace{\begin{bmatrix}1 & 0\\ b_{21} & b_{22}\\ b_{31} & b_{32}\\ 0 & 1\end{bmatrix}}_{\mathbf{B}^{\mathrm{T}}} \underbrace{\begin{bmatrix}\omega_c\\ \omega_r\end{bmatrix}}_{\mathbf{x}=\mathbf{y}_r} \quad \Rightarrow \quad \begin{bmatrix}\omega_t\\ \omega_s\end{bmatrix} = \begin{bmatrix}b_{21} & b_{22}\\ b_{31} & b_{32}\end{bmatrix}\begin{bmatrix}\omega_c\\ \omega_r\end{bmatrix}. \tag{E.1}$$

In steady-state condition, the static input–output relation of system (32) is $\mathbf{y} = \overline{\mathbf{H}}_0\mathbf{u}$ where $\overline{\mathbf{H}}_0 = -\mathbf{B}^{\mathrm{T}}\mathbf{A}^{-1}\mathbf{B} \in \mathcal{R}^{(4\times4)}$ is a matrix of rank 2, see (33). When $\mathbf{y} \in \mathrm{Im}(\mathbf{B}^{\mathrm{T}})$, the set $\tilde{\mathbf{u}}$ of all the solutions $\mathbf{u}$ of relation $\mathbf{y} = \overline{\mathbf{H}}_0\mathbf{u}$ is $\tilde{\mathbf{u}} = \mathbf{u}_0 + \ker(\mathbf{B})$ where $\mathbf{u}_0$ is a particular solution. The minimum norm solution $\mathbf{u}$ of set $\tilde{\mathbf{u}}$ satisfies the conditions given in (D.3): $\mathbf{u} \in \ker(\mathbf{B})^{\perp} = \mathrm{Im}(\mathbf{B}^{\mathrm{T}})$. From (D.3), it follows that the minimum norm solution $\mathbf{u}$ can be expressed as follows:

$$\underbrace{\begin{bmatrix}T_c\\ T_t\\ T_s\\ T_r\end{bmatrix}}_{\mathbf{u}} = \underbrace{\begin{bmatrix}1 & 0\\ b_{21} & b_{22}\\ b_{31} & b_{32}\\ 0 & 1\end{bmatrix}}_{\mathbf{B}^{\mathrm{T}}} \underbrace{\begin{bmatrix}T_c\\ T_r\end{bmatrix}}_{\mathbf{u}_r} \quad \Rightarrow \quad \begin{bmatrix}T_t\\ T_s\end{bmatrix} = \begin{bmatrix}b_{21} & b_{22}\\ b_{31} & b_{32}\end{bmatrix}\begin{bmatrix}T_c\\ T_r\end{bmatrix}. \tag{E.2}$$

Relation (E.2) is an algebraic constraint between the components $T_c$, $T_t$, $T_s$ and $T_r$ of the input vector $\mathbf{u}$.

## References


[1] C.B. Yan, Q. Zhao, Analytical approach to estimate efficiency of series machines in production lines, IEEE Trans. Autom. Sci. Eng. 15 (3) (2018) 1027–1040, http://dx.doi.org/10.1109/TASE.2017.2702380.

[2] R. Zanasi, The power-oriented graphs technique: system modeling and basic properties, in: IEEE Vehicle Power and Propulsion Conference (VPPC), 2010, http://dx.doi.org/10.1109/VPPC.2010.5729018.

[3] P.R. Ouyang, Q. Li, W.J. Zhang, L.S. Guo, Design, Modeling and control of a hybrid machine system, Mechatronics 14 (10) (2004) 1197–1217, http://dx.doi.org/10.1016/j.mechatronics.2004.06.004.

[4] W.J. Zhang, P.R. Ouyang, Z.H. Sun, A novel hybridization design principle for intelligent mechatronics systems, in: International Conference on Advanced Mechatronics, 2010, http://dx.doi.org/10.1299/jsmeicam.2010.5.67.

[5] J.R. Senft, Mechanical efficiency of kinematic heat engines, J. Franklin Inst. 324 (2) (1987) 273–290, http://dx.doi.org/10.1016/0016-0032(87)90066-4.

[6] J.R. Senft, General analysis of the mechanical efficiency of reciprocating heat engines, J. Franklin Inst. 330 (5) (1993) 967–984, http://dx.doi.org/10.1016/0016-0032(93)90088-C.

[7] F. Farhani, A. Zaafouri, A. Chaari, Real time induction motor efficiency optimization, J. Franklin Inst. 354 (8) (2017) 3289–3304, http://dx.doi.org/10.1016/j.jfranklin.2017.02.012.

[8] M.L. Corradini, G. Ippoliti, G. Orlando, Fault-tolerant sensorless control of wind turbines achieving efficiency maximization in the presence of electrical faults, J. Franklin Inst. 355 (5) (2018) 2266–2282, http://dx.doi.org/10.1016/j.jfranklin.2018.01.003.

[9] S.A. Evangelou, M.A. Rehman-Shaikh, Comprehensive energy efficiency analysis of series hybrid electric vehicles with dual-phase-shift-controlled DC-DC converter, J. Franklin Inst. 357 (13) (2020) 8761–8799, http://dx.doi.org/10.1016/j.jfranklin.2020.04.059.

[10] S.S. Williamson, A. Emadi, K. Rajashekara, Comprehensive efficiency modeling of electric traction motor drives for hybrid electric vehicle propulsion applications, IEEE Trans. Veh. Technol. 56 (4) (2007) 1561–1572, http://dx.doi.org/10.1109/TVT.2007.896967.

[11] W. Yang, J. Liang, J. Yang, P.D. Walker, N. Zhang, Corresponding drivability control and energy control strategy in uninterrupted multi-speed mining trucks, J. Franklin Inst. 358 (2) (2021) 1214–1239, http://dx.doi.org/10.1016/j.jfranklin.2020.11.014.

[12] J.M. Miller, Hybrid electric vehicle propulsion system architectures of the e-CVT type, IEEE Trans. Power Electron. 21 (3) (2006) 756–767, http://dx.doi.org/10.1109/TPEL.2006.872372.

[13] J. Liu, H. Peng, Modeling and control of a power-split hybrid vehicle, IEEE Trans. Control Syst. Technol. 16 (6) (2008) 1242–1251, http://dx.doi.org/10.1109/TCST.2008.919447.

[14] G. Wu, X. Zhang, Z. Dong, Powertrain architectures of electrified vehicles: review, classification and comparison, J. Franklin Inst. 352 (2) (2015) 425–448, http://dx.doi.org/10.1016/j.jfranklin.2014.04.018.

[15] D. Tebaldi, R. Zanasi, Modeling and control of a power-split hybrid propulsion system, in: IEEE 45th Annual Conference of the Industrial Electronics Society (IECON), 2019, http://dx.doi.org/10.1109/IECON.2019.8927084.

[16] M. Bidarvatan, M. Shahbakhti, Analysis and control of torque split in hybrid electric vehicles by incorporating powertrain dynamics, J. Dyn. Syst. Meas. Control 140 (11) (2018) 111009, http://dx.doi.org/10.1115/1.4040219.

[17] K. Li, F.-C. Chou, J.-Y. Yen, Real-time, energy-efficient traction allocation strategy for the compound electric propulsion system, IEEE/ASME Trans. Mechatronics 22 (3) (2017) 1371–1380.

[18] J. Wu, J. Liang, J. Ruan, N. Zhang, P.D. Walker, A robust energy management strategy for EVs with dual input power-split transmission, Mech. Syst. Signal Process. 111 (2018) 442–455, http://dx.doi.org/10.1016/j.ymssp.2018.04.007.

[19] W. Junnian, W. Jun, W. Qingnian, Z. Xiaohua, Control rules extraction and parameters optimization of energy management for bus series-parallel AMT hybrid powertrain, J. Franklin Inst. 355 (5) (2018) 2283–2312, http://dx.doi.org/10.1016/j.jfranklin.2017.12.039.

[20] K. Shi, X. Li, Efficiency improvement of electrically activated rotation-flow suction unit based on drag torque and suction force modeling, IEEE Trans. Mechatronics 25 (2) (2020) 882–893, http://dx.doi.org/10.1109/TMECH.2019.2961176.

[21] L.H. Manring, N.D. Manring, Mapping the efficiency of a double acting, single-rod hydraulic-actuator using a critically centered four-way spool valve and a load-sensing pump, J. Dyn. Syst. Meas. Control 140 (9) (2018) 091017, http://dx.doi.org/10.1115/1.4039572.

[22] Y. Iino, Consideration on systematic analysis and evaluation of energy system efficiency, in: SICE Annual Conference, 2011.

[23] Z. Shijian, K. Xiangyu, L. Ye, Q. Yanan, D. Delong, Energy efficiency evaluation system based on ladder-based comprehensive assessment method, in: China International Conference on Electricity Distribution (CICED), 2018, http://dx.doi.org/10.1109/CICED.2018.8592514.

[24] A. Rassõlkin, H. Heidari, A. Kallaste, T. Vaimann, J. Pando Acedo, E. Romero-Cadaval, Efficiency map comparison of induction and synchronous reluctance motors, in: 26th International Workshop on Electric Drives: Improvement in Efficiency of Electric Drives (IWED), 2019, http://dx.doi.org/10.1109/IWED.2019.8664334.
[25] V.H.B. Manne, A. Vacca, K. Merrill, A numerical method for evaluating the torque efficiency of hydraulic orbit motors considering deformation effects and frictional losses, Mech. Syst. Signal Process. 146 (2021) http://dx.doi.org/10.1016/j.ymssp.2020.107051.
[26] X. Yang, G. Gong, H. Yang, L. Jia, J. Zhou, An investigation in performance of a variable-speed-displacement pump-controlled motor system, IEEE Trans. Mechatronics 22 (2) (2017) 647–656, http://dx.doi.org/10.1109/TMECH.2016.2544440.
[27] M. Li, R. Foss, K.A. Stelson, J.D. Van de ven, E.J. Barth, Design, dynamic modeling, and experimental validation of a novel alternating flow variable displacement hydraulic pump, IEEE Trans. Mechatronics 24 (3) (2019) 1294–1305, http://dx.doi.org/10.1109/TMECH.2019.2906859.
[28] X. Roboam, Systemic Design Methodologies for Electrical Energy Systems: Analysis, Synthesis and Management, ISTE Willey Editions, ISBN: 978-1-118-56967-2, 2012.
[29] S. Lichiardopol, C. Sueur, Duality in system analysis for bond graph models, J. Franklin Inst. 347 (2) (2010) 377–414, http://dx.doi.org/10.1016/j.jfranklin.2008.10.002.
[30] K. Li, A. Bouscayrol, S. Han, S. Cui, Comparisons of electric vehicles using modular cascade machines system and classical single drive electric machine, IEEE Trans. Veh. Technol. 67 (1) (2018) 354–361, http://dx.doi.org/10.1109/TVT.2017.2743216.
[31] R. Zanasi, POG modeler: the web power-oriented graphs modeling program, IFAC-PapersOnLine 53 (2) (2020) 13030–13035, http://dx.doi.org/10.1016/j.ifacol.2020.12.2171.
[32] R. Zanasi, G.H. Geitner, A. Bouscayrol, W. Lhomme, Different energetic techniques for modelling traction drives, in: 9th International Conference on Modeling and Simulation of Electric Machines, Converters and Systems (ELECTRIMACS), 2008.
[33] R. Zanasi, D. Tebaldi, Planetary gear modeling using the power-oriented graphs technique, in: IEEE European Control Conference (ECC), 2019, http://dx.doi.org/10.23919/ECC.2019.8796006.
[34] R. Zanasi, D. Tebaldi, Modeling of complex planetary gear sets using power-oriented graphs, IEEE Trans. Veh. Technol. 69 (12) (2020) 14470–14483, http://dx.doi.org/10.1109/TVT.2020.3040899.
[35] D. Tebaldi, R. Morselli, R. Zanasi, Estimation of physical parameters using a new discrete-time derivative algorithm, IFAC-PapersOnLine 53 (2) (2020) 2367–2372, http://dx.doi.org/10.1016/j.ifacol.2020.12.033.
[36] Y. Su, M. Hu, L. Su, D. Qin, T. Zhang, C. Fu, Dynamic coordinated control during mode transition process for a compound power-split hybrid electric vehicle, Mech. Syst. Signal Process. 107 (2018) 221–240, http://dx.doi.org/10.1016/j.ymssp.2018.01.023.
[37] H.L. Benford, M.B. Leising, The lever analogy: a new tool in transmission analysis, SAE Trans. 90 (1) (1981) 429–437, http://dx.doi.org/10.4271/810102.
[38] C.H. Hsu, A graph notation for the kinematic analysis of differential gear trains, J. Franklin Inst. 329 (5) (1992) 859–867, http://dx.doi.org/10.1016/S0016-0032(92)90044-H.
[39] C.H. Hsu, A graph representation for the structural synthesis of geared kinematic chains, J. Franklin Inst. 330 (1) (1993) 131–143, http://dx.doi.org/10.1016/0016-0032(93)90025-P.
[40] C.H. Hsu, Synthesis of kinematic structure of planetary gear trains by admissible graph method, J. Franklin Inst. 330 (5) (1993) 913–927, http://dx.doi.org/10.1016/0016-0032(93)90085-9.
[41] R. Zanasi, D. Tebaldi, Power flow efficiency of linear and nonlinear physical systems, in: IEEE European Control Conference (ECC), 2019, http://dx.doi.org/10.23919/ECC.2019.8796275.
[42] R. Zanasi, D. Tebaldi, Study of the bidirectional efficiency of linear and nonlinear physical systems, in: IEEE 45th Annual Conference of the Industrial Electronics Society (IECON), 2019, http://dx.doi.org/10.1109/IECON.2019.8927686.